Bistability in superconducting rings containing an inhomogeneous Josephson junction

M. Gaass,[1] S. Nadj-Perge,[2,*] Z. Radović,[2] A. Bauer,[1] M. Aprili,[3] W. Wegscheider,[1] and C. Strunk[1]
[1]*Institute for Experimental and Applied Physics, University of Regensburg, 93025 Regensburg, Germany*
[2]*Department of Physics, University of Belgrade, P.O. Box 368, 11001 Belgrade, Serbia*
[3]*Laboratoire de Physique des Solides, CNRS, UMR 8502, Université Paris-Sud, 91405 Orsay Cedex, France*
(Received 26 October 2007; published 11 January 2008)

We investigate the magnetic response of a superconducting Nb ring containing a ferromagnetic PdNi Josephson junction and a tunnel junction in parallel. Doubling of the switching frequency is observed within certain intervals of the external magnetic field. For sinusoidal current-phase relations in both junctions, our model of a double superconducting quantum interference device (a small two-junction loop that interrupts the larger ring) explains this feature by a sequence of current reversals in the ferromagnetic section of the junction in these field intervals. The switching anomalies are induced by the coupling between the magnetic fluxes in the two superconducting loops.

DOI: 10.1103/PhysRevB.77.024506 PACS number(s): 85.25.Dq

I. INTRODUCTION

A superconducting quantum interference device (SQUID) consists of a superconducting loop interrupted by one or two Josephson junctions. They are usually referred to as rf and dc-SQUIDs, respectively, due to the standard biasing modes of operation (radio frequency or direct current). The magnetic moment of rf SQUIDs and the critical current of dc-SQUIDs are periodic functions of the magnetic flux Φ enclosed by the loop. In most cases, the periodicity is given by the magnetic flux quantum $\Phi_0=h/2e$. This is a consequence of the gauge-invariant connection between Φ and the phase difference φ across the junction(s) via the current-phase relation (CPR) $I_s(\varphi)$. Under certain conditions, the CPR of the junction(s) is not a simple sine, but it can contain higher harmonics: $I_s(\varphi)=\Sigma_n I_c^{(n)} \sin n\varphi$, where the coupling coefficients $I_c^{(n)}$ quantify the relative strength of processes with a coherent transfer of n Cooper pairs.[1] In some cases, the first order coefficient $I_c^{(1)}$ can even vanish, for instance, in asymmetric 45° grain boundary junctions in d-wave symmetry superconductors,[2,3] in out of equilibrium superconductor-normal-metal-superconductor junctions[4] and for ballistic superconductor-ferromagnet-superconductor (SFS) junctions at the 0-π transition.[5,6] The remaining second order coefficient $I_c^{(2)}$ will result in a doubling of the frequency in the interference pattern. Although, a frequency doubling has been observed experimentally,[7] its origin is still under debate, since there are also dynamic effects in inhomogeneous junctions, which can lead to this effect.[8,9]

Recently, it was observed that the critical current of high temperature superconductor dc-SQUIDs shows a $\Phi_0/2$ periodicity in certain sections of the interference pattern.[3] To explain this observation, it was suggested that the random faceting of the grain boundary induces a distribution of 0 and π couplings along the junction. For some particular values of the applied magnetic field, the first order coupling of the overall junction is zero, allowing second order coupling to be dominant. A similar effect has also been measured in the multiterminal transport of a two-dimensional electron gas connected to a superconducting loop.[10]

Here, we report on a different material system, showing a similar phenomenology, and suggest an alternative interpretation of this phenomenon. We study the magnetic response of an rf SQUID where the junction is inhomogeneous and formed by the parallel connection of a conventional (0) Josephson junction and a ferromagnetic π junction. By measuring the total flux in the SQUID while increasing the external magnetic field B_{ext}, we mostly observe a Φ_0-periodic penetration of flux quanta into the loop every time the critical current of the junction is exceeded. However, for some values of the external magnetic field, we find a doubling of the switching frequency. We propose the following double SQUID model: a large superconducting ring is interrupted by a small loop that contains two junctions. This model explains the effect in terms of a bistability of the supercurrent in the π junction for certain values of the applied magnetic field. The model also successfully explains the magnetic field and temperature dependence of our observations, even when the CPR of both junctions is assumed to be purely sinusoidal. SQUIDs with two quantization loops have already been studied[11] and used for the observation of resonant tunneling between macroscopically distinct quantum states.[12]

II. SAMPLE PREPARATION

We use Nb as the superconductor and dilute PdNi as the ferromagnet for our SFS junctions. To pattern the loops, we employ a robust Si_3N_4 and/or polyether sulfone (PES) mask system for shadow evaporation. The PES forms a highly thermostable sacrificial layer.[13] The 60 nm thick Si_3N_4 was deposited by plasma enhanced chemical vapor deposition on top of the PES and provides sufficient mechanical stability to resist the large stresses created by the Nb film. After patterning the mask by electron beam lithography and reactive ion etching using CHF_3, the Si_3N_4 mask was underetched by an isotropic oxygen plasma. The undercut can have a value of up to 1 μm. Evaporation of 40 nm of Nb and 10 nm of PdNi under different angles provides the desired superconducting loops with an integrated SFS planar junction, as illustrated by a scanning electron micrographs of a sample in Figs. 1(a) and 1(b). In Figs. 1(c) and 1(d), the equivalent schematics are shown. The thickness of the PdNi film was chosen to produce a π junction close to the 0-π crossover.[14] A 10%

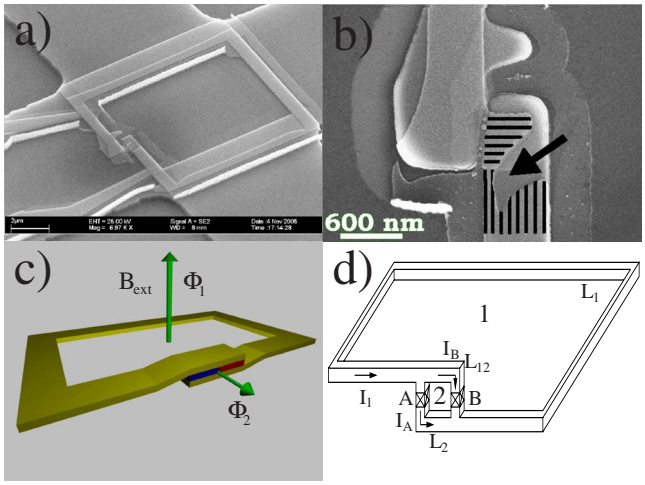

FIG. 1. (Color online) (a) Scanning electron image of the loop on top of the active area of the Hall sensor. Two leads connected on both sides of the junction are used to control the flux through the loop. (b) A zoom onto the junction area showing the parallel connection of the Nb/Nb contact (junction *A*, vertical lines) and the Nb/PdNi/Nb (junction *B*, horizontal lines). (c) Schematic of the device geometry. (d) Schematic of the equivalent double SQUID: loops 1 and 2 with self-inductances L_1 and L_2 and mutual inductance L_{12} containing junctions *A* and *B*.

misalignment of the sample during evaporation of the second Nb layer resulted in an overlap of the two Nb films without PdNi interlayer, as indicated by the arrow in Fig. 1(b). Strong gettering of residual gas by the Nb during evaporation of PdNi results in a rather transparent tunneling contact between the two Nb films in this area, as a second Josephson junction.

III. EXPERIMENTAL RESULTS

We have placed the sample on top of the active area of a micron-sized Hall sensor in order to detect the magnetic response.[15,16] The Hall sensor is realized in a semiconductor heterostructure having the electron density of 2.25×10^{15} m^{-2} and the mobility of 1.13×10^{6} cm^2/V s. We achieve a sensitivity of roughly 500–50 nT/Hz$^{1/2}$ depending on the sensor current. For our loop dimensions of approximately 7.6×8.5 μm^2, the magnetic flux quantum $\Phi_0=2.067\times10^{-15}$ V s corresponds to a magnetic field of about 31 μT.

Upon sweeping the external magnetic field, circulating supercurrents in the sample are generated. The resulting flux in the Nb ring Φ_1 induces a flux-periodic contribution to the Hall voltage across the Hall sensor, while the contribution of the external flux Φ_{e1} is simply subtracted. A typical trace of the induced flux $\Phi_1-\Phi_{e1}$ vs Φ_e is depicted for two different temperatures in Fig. 2(a). Only the flux through the ring is measured due to negligible contribution of the almost orthogonally tilted microloop [see Fig. 1(c)]. The magnetic response of the ring is strongly hysteretic due to the large LI_c product; the latter is characterized by the parameter $\beta_{L1}=2\pi L_1 I_{c1}/\Phi_0 \gg 1$.[17] The ring inductance is determined

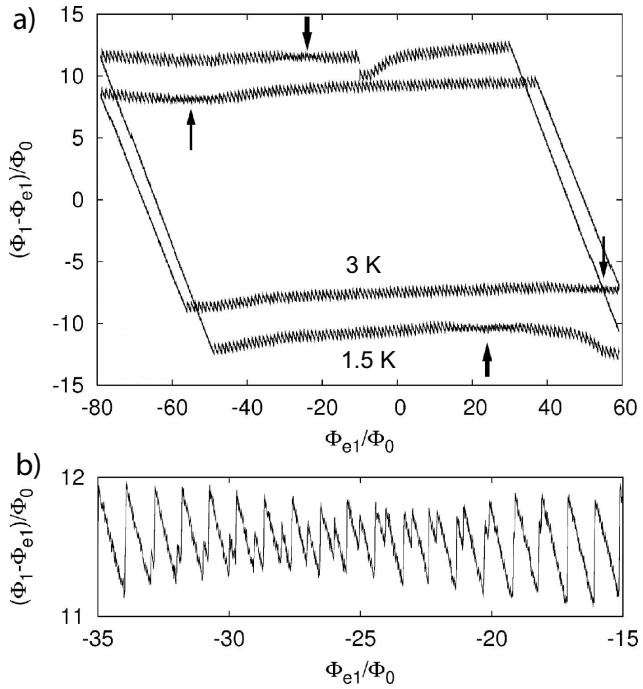

FIG. 2. (a) Full hysteresis cycle for two different temperatures, $T=1.5$ K (outer cycle) and 3.0 K (inner cycle), corresponding to the critical currents $I_{c1}\simeq980$ and 690 μA, respectively. The arrows indicate positions of substructures with double frequency. With increasing temperature, the substructures are shifted to higher fields. The ring inductance $L_1\simeq26$ *p*H is determined from the estimated filling factor of the magnetometer. The irregular drifts and jumps are artifacts of the Hall cross. (b) Magnified top substructure on outer cycle is shown as an example (all other substructures are similar). The absolute value of the induced flux $\Phi_1-\Phi_{e1}$ is determined from the jump height with an uncertainty of $0.1\Phi_0$.

from the estimated filling factor of the magnetometer. The critical current is determined from the vertical size of the hysteresis loops in Fig. 2(a).

The signal shows the additional substructures in the switching pattern in certain intervals of the external magnetic field, as indicated by the arrows in Fig. 2(a). This effect has been seen in three samples with similar inhomogeneous junction geometry. A zoom onto the top substructure in the outer cycle is shown in Fig. 2(b). All other substructures are similar. It can be seen that the regular Φ_0-periodic switching pattern is interrupted by additional peaks, which gain height, until they take over. The field intervals displaying the substructure in the switching behavior shift toward higher field when the temperature is increased. The observed substructure is not the predicted frequency doubling effect, expected for a dominant second harmonic contribution to the CPR.[6] As we show below, it can be explained in terms of two coupled loops, even for a sinusoidal CPR of both 0 and π junctions.

IV. MODEL CALCULATIONS

In the following model treatment, we approximate the extended inhomogeneous junction by a parallel connection of

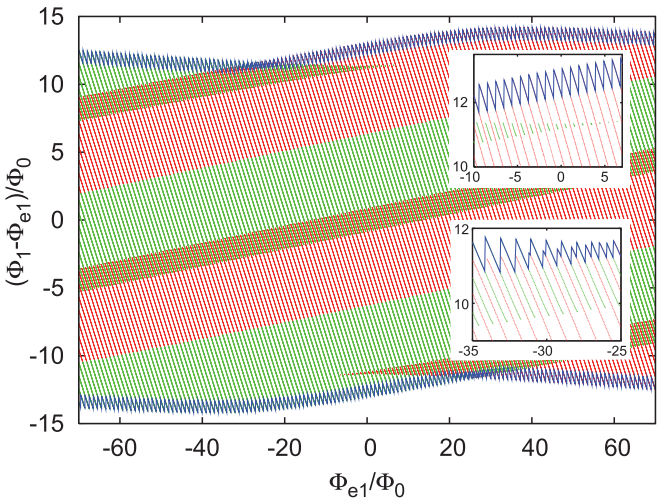

FIG. 3. (Color) The map of local energy minima of the double SQUID. Red and green lines correspond to positive and negative signs of the current I_B. Top and bottom sawtooth lines represent the largest hysteresis in $\Phi_1-\Phi_{e1}$. Parameters are the same as in Fig. 4 (outer cycle). Upper inset: nucleation of states with opposite I_B (green). Lower inset: alternation of states (red and green lines) with positive and negative signs of I_B in the region with frequency doubling.

two short junctions A and B, the latter being in the π state. We assume a sinusoidal current-phase relations $I_{A(B)}=I_{cA(B)}\sin\varphi_{A(B)}$. These two junctions form a small loop with an inductance L_2, which interrupts the large loop with inductance L_1. Our double SQUID model with two quantization loops is sketched in Fig. 1(d). The supercurrents circulating in the two SQUID loops are coupled by the Kirchhoff laws and their mutual inductance L_{12}.

The free energy of the circuit is given by

$$W=E_A(\varphi_A)+E_B(\varphi_B)+\frac{1}{2}L_1I_1^2+\frac{1}{2}L_2I_2^2+L_{12}I_1I_2, \quad (1)$$

where φ_A and φ_B are the macroscopic phase differences across the junctions A and B, $I_1=I_A+I_B$ is the current circulating in the large loop, and $I_2=I_A$ is the current circulating in the small loop, where I_A and I_B are the currents through junctions A and B, respectively. The first two terms in Eq. (1) are the Josephson energies $E_i(\varphi_i)=(\Phi_0/2\pi)|I_{ci}|(1\mp\cos\varphi_i)$ $(i=A,B)$ for 0 and π junctions, respectively. The three remaining terms represent the magnetostatic energy.[17,18] The magnetic fluxes Φ_1 and Φ_2 through the loops 1 and 2 are given by

$$\Phi_1=\Phi_{e1}-L_1I_1-L_{12}I_2, \quad \Phi_2=\Phi_{e2}-L_{12}I_1-L_2I_2. \quad (2)$$

Here, Φ_{e1} and Φ_{e2} are the corresponding fluxes of the external magnetic field. The total fluxes are related to the phase differences,

$$\Phi_1=\frac{\Phi_0}{2\pi}\varphi_B, \quad \Phi_2=\frac{\Phi_0}{2\pi}(\varphi_A-\varphi_B). \quad (3)$$

Finally, Eq. (1) can be rewritten explicitly as a function of Φ_1 and Φ_2 in the form

$$W=E_A(\varphi_A)+E_B(\varphi_B)+\frac{1}{L_1L_2-L_{12}^2}\left[\frac{L_2}{2}(\Phi_1-\Phi_{e1})^2+\frac{L_1}{2}(\Phi_2-\Phi_{e2})^2-L_{12}(\Phi_1-\Phi_{e1})(\Phi_2-\Phi_{e2})\right]. \quad (4)$$

For given external fluxes Φ_{e1} and Φ_{e2}, the local minima of the free energy W with respect to Φ_1 and Φ_2 are calculated numerically and plotted in Fig. 3. Like for usual rf SQUIDs in the hysteretic regime, the circulating current in the large loop is a multivalued function of external flux if $\beta_{L_1}>1$. When the external magnetic field is swept, e.g., in negative direction, the circulating supercurrent follows the lines of local energy minima, as indicated by the red lines in Fig. 3. At the upper end of each line, the state becomes unstable and the system switches into the nearest available state with lower free energy, as reflected by the sharp drops in Φ_1. The envelope of these jumps is periodic due to a modulation of the maximum I_1 by the integrated dc-SQUID. This comes from the coupling between Φ_1 and Φ_2, implying a circulating current also in the small loop (e.g., with $I_B>0$), which contributes to the free energy. Around $\Phi_{e1}/\Phi_0\approx 5$, states with opposite current I_B in the small junction become stable (see the short green lines in the upper inset of Fig. 3). The stability region for this set of states grows until they eventually become more stable than those with the original (positive) orientation of I_B. This is precisely the region, where these states become involved in the switching process. In this region, states with positive and negative orientations of the current in the small loop alternate, resulting in a doubling of the switching frequency (lower inset of Fig. 3). When the external flux is decreased further, the states with the positive orientation of I_B become energetically unfavorable and their region of stability shrinks, until the switching processes entirely involve states with negative I_B (green lines). In this way, the doubling of the switching frequency is traced back not to a period doubling in the CPR but to the presence of the twofold orientation of the current in the π section of the junction. If the CPR contains a significant amount of second harmonics, an additional $\Phi_0/2$-*periodic* fine structure is expected in the switching pattern.

V. COMPARISON BETWEEN THEORY AND EXPERIMENT

To compare the numerical results with our experiment, we take junction A in the 0 state (tunnel junction, $I_{cA}>0$) and junction B in the π state (SFS, $I_{cB}<0$), and $I_{cA}/I_{cB}=-10$, $\beta_{L_1}=90$, $\beta_{L_2}=2\pi L_2I_{cB}/\Phi_0=-1.5$, $2\pi L_{12}I_{cA}/\Phi_0=-9.7$, and $\Phi_{e2}/\Phi_{e1}=-0.005$. The critical current I_{cA} and inductance of the ring L_1 are determined directly from the experimental hysteresis loop in Fig. 2(a), while I_{cB} is estimated from previous measurements on similar Nb-PdNi junctions.[15] The inductance L_2 and mutual inductance L_{12} affect mainly the size and position of the switching anomaly on the hysteresis loop. For reasonable values of chosen parameters, a good agreement is achieved between the experimental data for $T=1.5$ K and numerical simulations (see Figs. 2 and 4). Note that the ratio Φ_{e2}/Φ_{e1} of external fluxes differs from the loop area ratio and has (for this sample) negative sign due to the

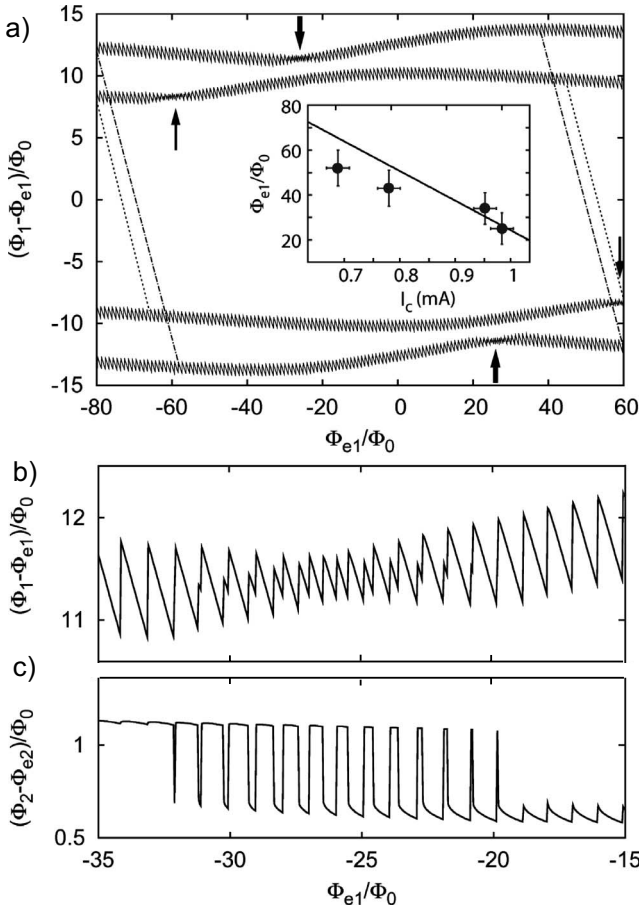

FIG. 4. (a) Calculated largest hysteretic cycles fitted to the experimental data shown in Fig. 2 with the parameters given in the text. The inner cycle corresponds to a reduction of I_{cA} and I_{cB} by 25%, corresponding to the higher temperature. The dotted lines correspond to the reversal of the sweep direction in the experiment. Inset: shift of the switching anomaly with the measured total critical current $I_C(T)$ at temperatures 3, 2.5, 2, and 1.5 K (dots). The solid line represents the theoretical prediction with the same set of parameters. (b) Zoom onto the upper substructure in the outer cycle. (c) Corresponding induced flux through the small loop.

almost orthogonal tilt of the small loop with respect to the sample. Its value determines the number of the observed double switching events, and it can be readily determined from the data.

If we assume that the measured reduction of I_{cA} to $\approx 75\%$ at $T=3$ K (see Fig. 4) is similar also in $|I_{cB}|$, we can well reproduce the observed shift of the switching anomaly toward higher external flux [inner trace in Fig. 4(a)]. The dots in the inset of Fig. 4(a) show the measured shift of the switching anomaly vs the critical current $I_C(T)$ for different temperatures. The solid line represents theoretical results.

Sequences of the frequency doubling in the flux modulation periodically occur in certain intervals of the external magnetic field if $|\beta_{L_2}| \gtrsim 1$ of the smaller loop is sufficiently large. A zoom onto the substructure is shown in Fig. 4(b). Substructures in the switching pattern $\Phi_1 - \Phi_{e1}$ occur with the period $|\Phi_{e1}/\Phi_{e2}|$. The corresponding flux modulation in the small loop is shown in Fig. 4(c). When the external magnetic field is varied, small periodic perturbations induced by the large loop alternate periodically the energies of the two opposite current directions in the small loop, thus forming the bistable region with large flux oscillations [Fig. 4(c)]. The bistable region is placed symmetrically around the external flux value corresponding approximately to integer number of Φ_0 in the small loop and equal energies for opposite currents in the junction B.

Additional calculations show that in the ground state, the first substructure occurs in the low external field corresponding to $\Phi_{e2} \approx 0$. When both junctions are 0 junctions, the first substructure in the ground state is located at $\Phi_{e2} \approx \Phi_0/2$, which corresponds in our case to a very large Φ_{e1}. However, positions of substructures on the hysteretic loop are strongly shifted from the ground state values and depend on the mutual inductance. Numerical calculations show that practically the same hysteretic behavior shown in Fig. 4 can be obtained for junctions A and B both in the 0 state with similar parameters of the double SQUID.[19]

VI. CONCLUSIONS

To conclude, we have studied an rf SQUID containing an inhomogeneous Josephson junction as a weak link. We have found experimentally a doubling of the switching frequency in certain intervals of the external magnetic field. The inhomogeneous junction can be modeled as a small dc-SQUID with 0 and π Josephson junctions. This double SQUID model explains the observed switching anomaly by a bistable switching of the orientation of the current in the weaker section of the junction. The suggested mechanism is effective, independent of the shape of the CPR in both junctions, and may also be relevant for similar observations in other systems.

ACKNOWLEDGMENTS

We thank M. Reinwald for help with the preparation of the GaAs/AlGaAs heterostructures. This work has been supported by the German Science Foundation within SFB 689, the Serbian Ministry of Science under Project No. 141014, the Franco-Serbian PAI EGIDE under Project No. 11049XG, and U.S. DOE under Project No. MA-509-MACA.

*Present address: Kavli Institute of Nanoscience, Delft University of Technology, P.O. Box 5046, 2600 GA Delft, the Netherlands.

[1] A. Golubov, M. Kupriyanov, and E. Il'ichev, Rev. Mod. Phys. **76**, 411 (2004).
[2] C. W. Schneider, G. Hammerl, G. Logvenov, T. Kopp, J. R. Kirtley, P. J. Hirschfeld, and J. Mannhart, Europhys. Lett. **68**, 86 (2004).
[3] T. Lindström, J. Johansson, T. Bauch, E. Stepantsov, F. Lombardi, and S. A. Charlebois, Phys. Rev. B **74**, 014503 (2006).
[4] J. J. A. Baselmans, T. T. Heikkilä, B. J. van Wees, and T. M. Klapwijk, Phys. Rev. Lett. **89**, 207002 (2002).
[5] Z. Radović, N. Lazarides, and N. Flytzanis, Phys. Rev. B **68**, 014501 (2003).
[6] Z. Radović, L. Dobrosavljević-Grujić, and B. Vujičić, Phys. Rev. B **63**, 214512 (2001).
[7] H. Sellier, C. Baraduc, F. Lefloch, and R. Calemczuk, Phys. Rev. Lett. **92**, 257005 (2004).
[8] S. M. Frolov, D. J. Van Harlingen, V. V. Bolginov, V. A. Oboznov, and V. V. Ryazanov, Phys. Rev. B **74**, 020503(R) (2006).
[9] M. Moshe and R. G. Mints, Phys. Rev. B **76**, 054518 (2007).
[10] S. G. den Hartog, C. M. A. Kapteyn, B. J. van Wees, T. M. Klapwijk, and G. Borghs, Phys. Rev. Lett. **77**, 4954 (1996).
[11] G. S. Krivoy and H. Koch, J. Appl. Phys. **74**, 2925 (1993).
[12] R. Rouse, S. Han, and J. E. Lukens, Phys. Rev. Lett. **75**, 1614 (1995).
[13] P. Dubos, P. Charlat, Th. Crozes, P. Paniez, and B. Pannetier, J. Vac. Sci. Technol. B **18**, 122 (2000).
[14] T. Kontos, M. Aprili, J. Lesueur, F. Genêt, B. Stephanidis, and R. Boursier, Phys. Rev. Lett. **89**, 137007 (2002).
[15] A. Bauer, J. Bentner, M. Aprili, M. L. Della Rocca, M. Reinwald, W. Wegscheider, and C. Strunk, Phys. Rev. Lett. **92**, 217001 (2004).
[16] A. K. Geim, S. V. Dubonos, J. G. S. Lok, I. V. Grigorieva, J. C. Maan, L. Theil Hansen, and P. E. Lindelof, Appl. Phys. Lett. **71**, 2379 (1997).
[17] A. Barone and G. Paterno, *Physics and Applications of the Josephson Effect* (Wiley, New York, 1982).
[18] L. D. Landau and E. M. Lifshitz, *Electrodynamics of Continuous Media*, Course of Theoretical Physics Vol. 8 (Pergamon, Oxford, 1980).
[19] S. Nadj-Perge and Z. Radović (unpublished).